Open Ceramics 5 (2021) 100055

Contents lists available at ScienceDirect

Open Ceramics

journal homepage: www.editorialmanager.com/oceram

Tuning of the high temperature behaviour of Si–C–N ceramics *via* the chemical crosslinking of poly(vinylmethyl-co-methyl)silazanes with controlled borane contents

Mélanie Wynn [a,**], David Lopez-Ferber [a], Antoine Viard [b], Diane Fonblanc [a], Marion Schmidt [a], Fabrice Rossignol [a], Pierre Carles [a], Georges Chollon [c], Christel Gervais [d], Samuel Bernard [a,*]

[a] Univ. Limoges, CNRS, IRCER, UMR 7315, F-87000, Limoges, France
[b] BJS Ceramics GmbH, Siemensstraße 6a L, D-86368, Gersthofen L, Germany
[c] University of Bordeaux, Laboratoire des Composites ThermoStructuraux (LCTS), UMR 5801: CNRS-Herakles(Safran)-CEA-UBx 3, Allée de La Boétie, 33600, Pessac, France
[d] Sorbonne Université, CNRS, Laboratoire de Chimie de La Matière Condensée de Paris, LCMCP, UMR 7574, F-75005, Paris, France

ARTICLE INFO

Keywords:
Si–B–C–N
Polysilazanes
Boron
Polymer derived ceramics
Crystallization

ABSTRACT

The thermal stability, elemental/phase composition evolution and crystallization behaviour of Si–B–C–N ceramics obtained by the pyrolysis of a series of poly (vinylmethyl-co-methyl)silazanes displaying various boron contents were investigated through annealing in the temperature range 1000–1800 °C under nitrogen atmosphere. The increase of the boron content in the early stage of the process involved the nucleation of β-SiC, inhibited the crystallization of α-Si_3N_4 and modified the activity of the sp^2-hybridised carbon phase in the derived ceramics obtained at 1000 and 1400 °C. At 1800 °C, low boron content Si–B–C–N ceramics gradually evolved toward a major SiC phase mainly formed via the carbothermal reaction of amorphous Si_3N_4 whereas high boron content Si–B–C–N ceramics led to highly stable materials with a complex microstructure made of SiC, Si_3N_4 and a BN-rich B(C)N phase that inhibited the activity of sp^2-hybridised carbon toward the carbothermal reaction of amorphous Si_3N_4 and significantly reduced the SiC crystallization process.

1. Introduction

There are usually two strategies to develop advanced high temperature ceramics. The first one consists in promoting the crystallinity of ceramics – in general by annealing at high temperature – in order to produce a crystalline structure that is stable at the temperature of application of the material. The second strategy focuses on the design of amorphous (non-crystalline) ceramics - using an appropriate combination of elements – that do not undergo nucleation and grain growth at the temperature of use [1]. This situation is particularly attractive as it suppresses the most important creep mechanism in ceramics, *i.e.*, grain boundary diffusion. This structural organization closely depends on the processing route which is applied to design such ceramics.

The application of the concept of 'better ceramics through chemistry", initially introduced by D. R. Ulrich [2], showed that tailoring the processing method through molecular engineering and precursor chemistry allows designing ceramics that could reach performances far beyond those developed by more conventional synthesis routes. A very convenient precursor route to produce such materials – especially in non-oxide ceramic systems – is the polymer derived ceramics (PDCs) route [3–8]. Such a method uses preceramic polymers as ceramic precursors, which are shaped and heat-treated into amorphous ceramics with a composition, microstructure [9–16] and shape [17–21] that have been determined at the polymer level [5,22]. Optionally (if the materials are not sufficiently thermally stable), an annealing process can be performed to crystallize the amorphous ceramics [16]. Alternatively, as-synthesized polymers can be directly pyrolysed into ceramic powders. Then, the latter can be shaped (*i.e.*, by sintering) to form the ceramics directly in the targeted shape [23–30].

The PDCs route has the advantage of producing stable amorphous ceramics which are prepared at (much) lower temperatures than for crystalline ceramics [31–34], which is of obvious interest in terms of

* Corresponding author.
** Corresponding author.
E-mail addresses: melanie.wynn@unilim.fr (M. Wynn), samuel.bernard@unilim.fr (S. Bernard).

https://doi.org/10.1016/j.oceram.2021.100055
Received 30 September 2020; Received in revised form 30 December 2020; Accepted 30 December 2020
Available online 6 January 2021
2666-5395/© 2021 The Authors. Published by Elsevier Ltd on behalf of European Ceramic Society. This is an open access article under the CC BY-NC-ND license (http://creativecommons.org/licenses/by-nc-nd/4.0/).

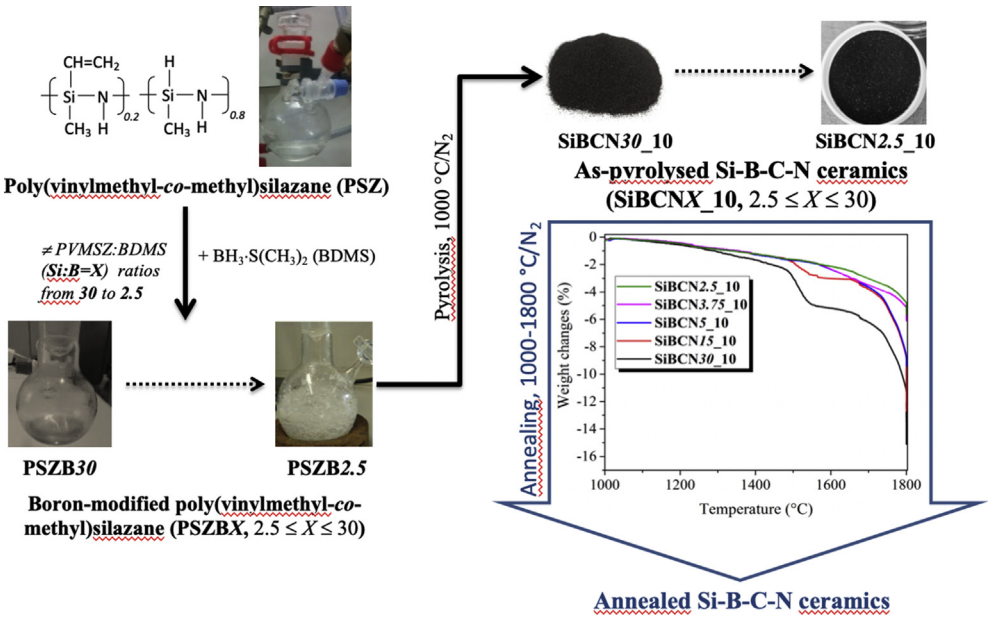

Fig. 1. Schematic diagram of the general process of designing Si–B–C–N ceramics from a series of boron-modified poly (vinylmethyl-co-methyl)silazanes displaying various boron contents with a special focus on annealing experiments.

energy consumption. However, their preparation as materials with high thermal and/or mechanical durability strongly depends on the choice of the element combinations and the nature of the chemical bonds, e.g. strong localized covalent bonds [1]. These requirements can be met by combining silicon (Si), carbon (C), nitrogen (N) and boron (B) at the atomic level in a single ceramic network [4,7,13,14,31,32,35–42]. The amorphous character of the covalent Si–B–C–N ceramics forms a specific metastable state, which occurs as an intermediate during the transformation of preceramic polymers into the final crystalline ceramics. Post-annealing of the amorphous compound at higher temperatures results in the crystallization of the corresponding thermodynamically stable crystalline phases, *i.e.*, B(C)N, SiC, Si_3N_4, C. The stability of the amorphous network is closely related to the chemistry and composition of the ceramic; thereby to the precursor chemistry.

In general, two different approaches are used to synthesize Si–B–C–N precursors. The first method relies on precursor blends of the desired composition and their thermal conversion (co-pyrolysis) into ceramics or the copolymerization of two precursors and their subsequent pyrolysis [41]. The second approach involves the synthesis of tailored *single-source* molecular compounds, which contain all the necessary elements desired in the ceramics, in a well-defined manner resulting in the homogeneous distribution of the various elements at the atomic scale [31,32,36]. The use of *single-source* precursors offers the advantages of producing high purity ceramics - the chemical synthesis of the polymers allows an easy purification of the reacting species by distillation or crystallization. It has been demonstrated that principally two ways may lead to the latter kind of molecular compounds. They are distinguished by the type of precursor used for their synthesis [35]. In the so-called "monomer route", a specifically designed monomer unit is polymerized. For example, an entity consisting of boron which is linked to $R_xSi(Cl)_{4-x}$ (R = H, CH_3 and/or $CH{=}CH_2$; $1 \leq x \leq 3$) units via C bridges is polymerized by ammonolysis, *i.e.* by treatment with ammonia (NH_3). In contrast, Si–B–C–N precursors obtained by the so-called "polymer route" are obtained by the chemical modification of a preformed polymer. A typical example is the attachment of B to a polysilazane bearing unsaturated hydrocarbons such as vinyl groups allowing hydroboration reactions using borane Lewis base adducts. The "polymer route" has numerous advantages: it offers a very high synthesis yield, the reaction is cheap, fast and does not create any side products [35,36]. Although rarely considered, this route appears to be promising, especially considering the commercial availability of polysilazanes at an affordable price. Indeed, polysilazanes - produced at an industrial scale and usually obtained by ammonolysis of chlorosilanes - can exhibit reactive functions that can further be used for the attachment of boron. Within this context, we recently published a detailed investigation of the chemical mechanisms involved in this type of synthesis procedure [42]. A commercially available poly (vinylmethyl-co-methyl)silazane (*Durazane*® 1800 by Merck) was reacted with different amounts of borane dimethylsulfide (BDMS) in order to induce hydroboration reactions of the vinyl groups. However, even if the reaction was conducted at 0 °C, BH groups interacted with the polysilazane's amino groups and dehydrocoupling reactions also occurred, leading to the formation of B–N bonds as confirmed by solid state NMR analyses. Incorporation of increasing boron contents was beneficial to the ceramic conversion mechanism, especially at low temperature, as it significantly enhanced the ceramic yield of the preceramic polymer. This synthesis strategy provided a very good control over the amount of borane added to the polysilazane and it enabled the fine control of the cross-linking degree of the polymer. This allowed us to optimize the viscosity and solubility of the preceramic polymer, for a processing in the liquid state (by impregnation) or in the solid state (by warm pressing), to obtain after pyrolysis at 1000 °C either porous or dense structures, depending on the boron content of the precursor [42]. Herein, these boron-modified poly (vinylmethyl-co-methyl)silazanes have been directly pyrolysed into ceramic powders with various boron contents up to 9 wt% at 1000 °C under nitrogen. These ceramics have been first characterised by elemental analyses and high-temperature thermogravimetric (TG) experiments before investigating their structural behaviour during annealing up to 1800 °C by Fourier transform infrared (FTIR), Raman and solid-state NMR spectroscopies, X-ray diffraction, and high-resolution TEM. In particular, we discussed the influence of the elemental and phase compositions of these Si–B–C–N ceramics on their structural and chemical behaviour (*e.g.*, nucleation, phase evolution, crystal growth and decomposition reactions) upon annealing to 1800 °C. Thus, a proper understanding of the amorphous-to-crystalline transformation of such ceramic powders with various and controlled Si:B ratios is provided. The schematic diagram of the general process of formation of Si–B–C–N ceramics from boron-modified poly (vinylmethyl-co-methyl)silazane, with a particular focus on the high temperature behaviour, is given in Fig. 1.

Table 1
Elemental composition of annealed samples measured by electron probe microanalyser (EPMA). Empirical formulas are referenced to $Si_{1.0}$ and normalized to 100 wt%.

Samples	Si ($_{wt}$%)	B ($_{wt}$%)	C ($_{wt}$%)	N ($_{wt}$%)	O ($_{wt}$%)	Chemical formula
SiBCN*15*_10	49.9	0.8	20.0	28.7	0.7	$Si_{1.0}B_{0.04}C_{0.9}N_{1.2}O_{0.02}$
SiBCN*5*_10	44.9	5.0	21.0	28.6	0.5	$Si_{1.0}B_{0.3}C_{1.1}N_{1.3}O_{0.02}$
SiBCN*2.5*_10	41.6	9.0	22.6	26.4	0.5	$Si_{1.0}B_{0.5}C_{1.3}N_{1.2}O_{0.02}$

2. Experimental

2.1. Materials

The synthesis of the precursors is carried out in a purified argon atmosphere passing through a column of phosphorus pentoxide and then a vacuum/argon line by means of standard Schlenk techniques. The cleaned glassware is stored in an oven at 90 °C overnight before being connected to the vacuum/argon line, assembled and pumped under vacuum for 30 min and then filled with argon. All chemical products are handled in an argon-filled glove box (Jacomex, Campus-type; O_2 and H_2O concentrations kept at $\leq$ 0.1 ppm and $\leq$0.8 ppm, respectively). Toluene (99.85%, Extra Dry over Molecular Sieve, AcroSeal(R)) was purchased from Acros Organics™. The poly (vinylmethyl-*co*-methyl) silazane (commercial name: Durazane® 1800) was provided by Merck company, Germany, stored in a fridge and used as received. It is labeled PSZ in the present paper. Anal. Found (wt%): Si, 41.3; C, 27.3; N, 22.7; H, 8.3; O, 0.4. $[Si_{1.0}C_{1.5}N_{1.1}H_{5.5}]_n$ (*Referenced to $Si_{1.0}$* and *oxygen content was omitted in the empirical formulae*). FTIR (ATR/cm^{-1}): ν(N–H) = 3388 (m), ν (C–H) = 3046 (s), 3010 (s), 2954 (s), 2895 (s), 2852 (m), ν(Si–H) = 2121 (vs), δ(vinyl) = 1591 (m), $\delta(CH_2)$ = 1405 (m), $\delta(Si–CH_3)$ = 1251 (s), δ (N–H): 1166 (m), δ (C–H + C–C + N–Si–N + Si–C) = 1005–630 (vs); ^{1}H NMR (300 MHz, $CDCl_3$, δ/ppm): 0.4–0.1 (br, $SiCH_3$), 1.1–0.5 (br, NH), 4.9–4.4 (br, SiH), 6.3–5.7 (br, vinyl). Borane dimethylsulfide $BH_3{\cdot}S(CH_3)_2$ solution (2.0 M of BDMS complex in toluene) was obtained from Acros Organics and used as received.

2.2. Precursor synthesis and thermochemical conversion into ceramic powders

The boron-modified PSZ samples labeled **PSZB*X*** with *X* corresponding to the Si:B molar ratio ($2.5 \leq X \leq 30$) have been synthesized by reacting controlled and various amount of BDMS with the commercially available PSZ, as described elsewhere [42]. Full characterisation of the polymers and pyrolysed derivatives has been done and results and discussions are described in ref. 42. Polymeric powders are placed in alumina boats in the glove-box, then put in a sealed tube under argon atmosphere to prevent any oxygen contamination of the samples during the transfer toward the furnace. Powders are transferred then introduced under argon flow into a silica tube inserted in a horizontal furnace (Carbolite BGHA12/450B). The tube is evacuated (0.1 mbar) and refilled with nitrogen (99.995%) to atmospheric pressure. Subsequently, the samples are subjected to a cycle of ramping of 5 °C.min^{-1} to 1000 °C in flowing nitrogen (dwelling time of 2 h). A constant flow (120 mL min^{-1}) is passed through the tube during the pyrolysis cycle. After cooling under nitrogen atmosphere, ceramic samples are obtained and they are labeled **SiBCN*X*_10** with *X* being the Si:B molar ratio ($2.5 \leq X \leq 30$) set for the corresponding precursor and 10 the first two digits of the pyrolysis temperature (1000 °C). They are subsequently placed in sintered vitreous carbon crucibles and then introduced in a graphite furnace (Nabertherm VHT-GR) for annealing treatments. The furnace is pumped under vacuum (1.10^{-1} mbar), refilled with nitrogen and maintained under a constant flow of gas (200 mL min^{-1}) during the whole heat treatment. The program consists of a 5 °C.min^{-1} heating ramp up to the maximum temperature fixed in the 1400–1800 °C range, dwelling at this temperature for 2 h, and cooling down to RT at 5 °C.min^{-1}. Samples are named as follows: **SiBCN*X*_T** with *X* being the Si:B molar ratio ($2.5 \leq X \leq 30$) set for the corresponding preceramic polymer and T the first two digits of the final annealing temperature, *e.g.*, 14 for an annealing temperature of 1400 °C.

2.3. Characterisation

High-temperature ThermoGravimetric Analyses (HTTGA) were performed on a Setsys Evolution TGA instrument from Setaram through heating up to 1800 °C at 5 °C/min using tungsten crucible and nitrogen as atmosphere. Elemental compositions (Si, B, N, O) of selected ceramic samples were determined using electron probe microanalyser (EPMA). Analyses were performed on a SC100 CAMECA device equipped with wavelength dispersive X-ray spectrometer (WDS). Measurements were carried out at 10 kV and 20 nA. Samples were polished and metallized prior to the analyses. Carbon content was then deduced. Some samples were characterised using an EDX (Oxford Aztec) detector on a SEM (Jeol IT 300 LV) apparatus. Three measurements done in different areas of the sample are averaged to give one result. Fourier-Transform Infrared (FT-IR) spectra were recorded on a ThermoFisher Nicolet nexus FT-IR device using an Attenuated Total Reflection (ATR) tool.

Solid-state ^{11}B and ^{29}Si NMR spectra were recorded on a Bruker AVANCE 700 and 300 spectrometers respectively (16.4 T: $\nu_0(^{11}B)$ = 224.63 MHz, 7.0 T: $\nu_0(^{29}Si)$ = 59.66 MHz) using 4 mm Bruker probes and spinning frequencies of 14 kHz and 10 kHz, respectively. Single pulse ^{29}Si MAS NMR spectra were recorded with a recycle delay of 60 s while ^{11}B MAS NMR spectra were acquired using a spin-echo θ-τ-2θ pulse sequence with $\theta = 90°$, to overcome problems related to the probe signal. The τ delay (71 μs) was synchronized with the spinning frequency and recycle delay was set to 2 s. Chemical shift values were referenced to tetramethylsilane for ^{29}Si and $BF_3{\cdot}OEt_2$ for ^{11}B. Raman spectroscopy was performed using a Renishaw InVia Reflex apparatus with a laser of λ = 532 nm; the program WIRE was used for the acquisition and treatment of the spectra. The global structure of samples has been determined by XRD analysis (Bruker AXS D8 Discover, CuK_α radiation). The scans were performed in the range of $2\theta \in \langle 20°; 90° \rangle$ with a step of 0.015° and an exposure time of 0.7 s. The diffraction patterns were analyzed using the Diffrac + EVA software with the JCPDS-ICDD database. Transmission Electronic Microscopy (TEM) was performed on a JEOL JEM 2100F apparatus. Selected samples were prepared by dispersing the grinded ceramic powder in water then letting a drop of this suspension evaporate on a selected support. ImageJ software was used to interpret the obtained images.

3. Results and discussion

After the pyrolysis of the **PSZB*X*** samples (*X* corresponds to the Si:B molar ratio set for the preceramic polymer, $2.5 \leq X \leq 30$) at 1000 °C in flowing nitrogen involving the polymer-to-ceramic conversion which has been investigated in our previous study [42], as-pyrolysed ceramic samples labeled **SiBCN*X*_10** ($2.5 \leq X \leq 30$) are obtained in yields changing from ca. 68% (**SiBCN*30*_10**) to ca. 82.5% (**SiBCN*2.5*_10**) [42]. In the first part of the present paper, as-pyrolysed ceramic samples displaying Si:B (= *X*) of 30 (**SiBCN*30*_10**), 15 (**SiBCN*15*_10**), 5, (**SiBCN*5*_10**) 3.75 (**SiBCN*3.75*_10**) and 2.5 (**SiBCN*2.5*_10**) as powders have been characterised by chemical analyses, XRD and FTIR/Raman spectroscopies before investigating their thermal behaviour by high temperature (1000–1800 °C) TG experiments.

Table 2
Calculated phase contents in selected samples based on elemental composition ($_{wt}$%, oxygen content has been neglected).

Samples	SiC ($_{wt}$%)	Si_3N_4 ($_{wt}$%)	C ($_{wt}$%)	BN ($_{wt}$%)
SiBCN*15*_10	14.5	68.5	15.2	1.8
SiBCN*5*_10	16.0	55.9	16.2	11.9
SiBCN*2.5*_10	27.4	38.3	15.8	18.8

3.1. Characterisation of elemental and phase composition of as-pyrolysed boron-modified Si–C–N ceramics

The bulk chemical analyses giving the empirical formula of selected samples provided in Table 1 (**SiBCN*15*_10**, **SiBCN*5*_10** and **SiBCN*2.5*_10**) show that the Si:B atomic ratio (from the calculated chemical formula) decreases from the **SiBCN*15*_10** sample to the **SiBCN*2.5*_10** sample in good agreement with the evolution of the Si:B atomic ratio fixed at the polymer level. This confirms that the composition of the powders can be adjusted in the early stage of the process, *i.e.*, at the atomic level in the polymer. Interestingly, it was possible to introduce a relatively high boron content, *i.e.*, 9.0 $_{wt}$% (13.6 $_{at}$%), in the ceramics with a Si:B ratio of 2.5 – because of the occurrence of hydroboration and dehydrocoupling reactions during the polymer synthesis - especially compared to Si–B–C–N ceramics which are generated from boron-modified polysilazanes [36,39,40]. The carbon content increased whereas the nitrogen content - relatively high compared to Si–B–C–N ceramics derived from the monomer [36] and polymer [39,40] routes - remained stable with the decrease of the Si:B.

Table 2 reports the calculation of the phase contents in the analyzed samples by considering the co-existence of SiC, Si_3N_4, C and BN as generally proposed for Si–B–C–N ceramics derived from boron-modified polysilazanes [36]. Note that we neglected the presence of silica because of the low oxygen content in ceramics.

As expected, samples with a high Si:B ratio consist of Si_3N_4 as a major phase, SiC, BN and free carbon as minor phases. The decrease of the Si:B ratio leads to the decrease of the Si_3N_4 phase portion by 40% while the SiC and especially the BN phase portions significantly increase. Based on the fact that the content of free carbon remains relatively stable, it can be concluded that the BN:C phase content ratio strongly increases with the decrease of the Si:B ratio. Such observations are in good agreement with the empirical formula ($Si_{1.0}C_{0.7}N_{0.9}O_{0.0}$) and the calculated phase content found in boron-free Si–C–N ceramics labeled **SiCN_10** (64.7 $_{wt}$% of Si_3N_4, 26.2 $_{wt}$% of SiC and 9.1 $_{wt}$% of free C) obtained through the pyrolysis of PSZ at 1000 °C in flowing nitrogen. Thus, we could deduce that the carbon phase content is significantly increased once boron is introduced in the samples while the Si_3N_4 phase content is relatively close. As a confirmation of the presence of free carbon in Si–B–C–N ceramics, the Raman spectra of as-pyrolysed samples (Fig. 2a) exhibit the bands of the defect-induced D (originates from the breathing mode A_{1g} of the sp^2 rings) and graphitic G bands (arises from the stretching mode E_{2g} of the sp^2 C–C bonds) at ~1355 cm^{-1} and ~1590 cm^{-1}, respectively. Considering that the D-mode is caused by a disordered structure in sp^2-hybridised carbon systems while the G band is characteristic of highly ordered

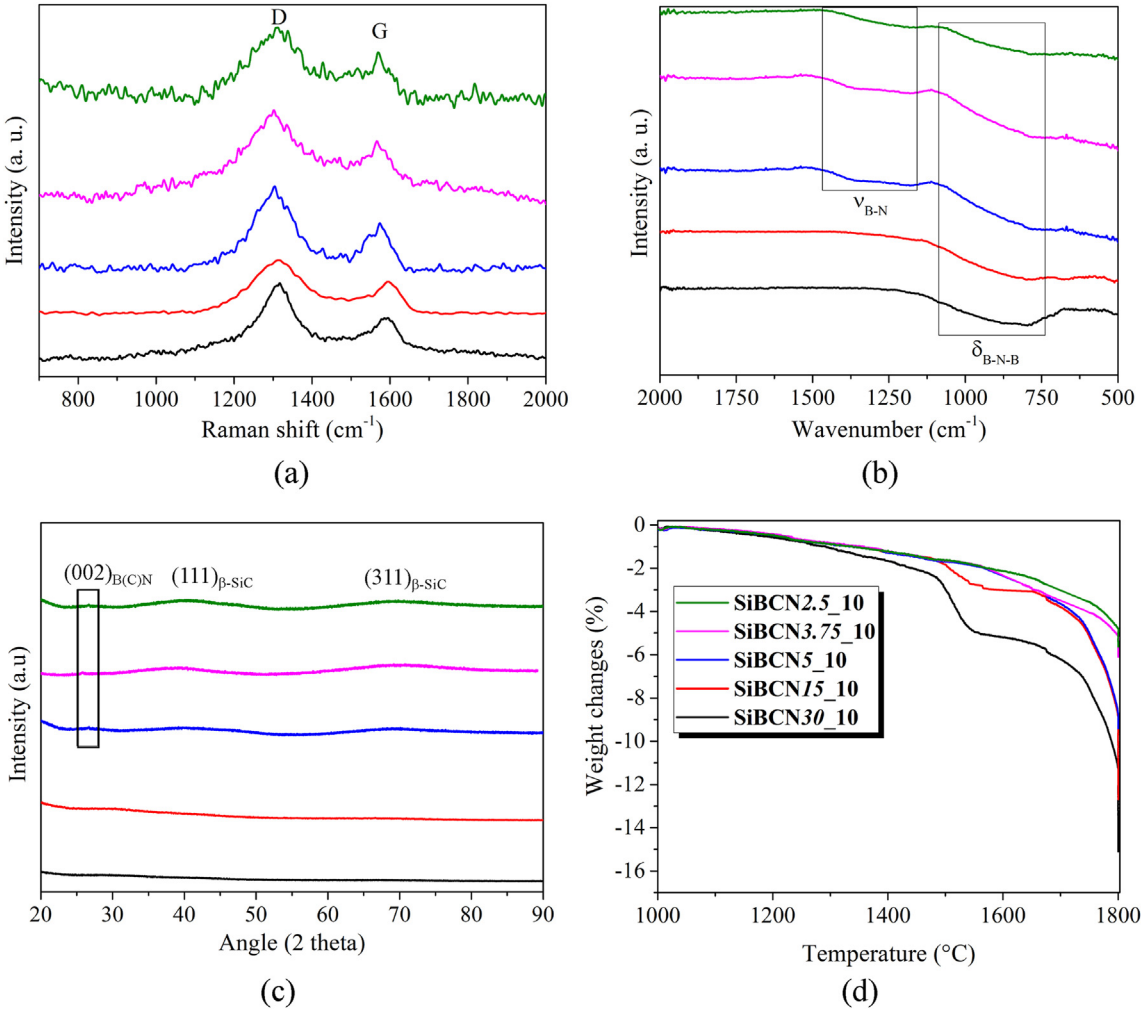

Fig. 2. Raman (a) and FTIR (b) spectra, XRD patterns (c) and TG curves (d) of as-pyrolysed samples with selected Si:B ratios.

Table 3
Elemental composition of annealed samples measured by electron probe microanalyser (EPMA) and EDS for samples with a star. Empirical formulas are referenced to $Si_{1.0}$ and normalized to 100 wt%. Oxygen values have been omitted in the determination of the chemical formula of samples because of a content below 2 $_{wt}$%.

Samples	Si ($_{wt}$%)	B ($_{wt}$%)	C ($_{wt}$%)	N ($_{wt}$%)	O ($_{wt}$%)	Chemical formula
SiBCN*15*_14	48.7	0.8	21.4	28.3	0.8	$Si_{1.0}B_{0.03}C_{1.0}N_{1.1}$
SiBCN*15*_16	53.0	1.4	18.7	26.5	0.4	$Si_{1.0}B_{0.07}C_{0.8}N_{1.0}$
SiBCN*15*_18*	68.6	1.2	28.5	1.0	0.7	$Si_{1.0}B_{0.04}C_{1.0}N_{0.03}$
SiBCN*5*_14	45.0	4.8	22.0	27.5	0.8	$Si_{1.0}B_{0.3}C_{1.1}N_{1.2}$
SiBCN*5*_16	50.0	3.3	19.2	27.2	0.4	$Si_{1.0}B_{0.2}C_{0.9}N_{1.1}$
SiBCN*5*_18*	67.9	4.6	25.4	1.8	0.2	$Si_{1.0}B_{0.2}C_{0.9}N_{0.07}$
SiBCN*2.5*_14	42.6	8.9	22.0	26.0	0.4	$Si_{1.0}B_{0.5}C_{1.2}N_{1.2}$
SiBCN*2.5*_16	44.0	8.5	21.2	25.9	0.4	$Si_{1.0}B_{0.5}C_{1.1}N_{1.2}$
SiBCN*2.5*_18*	48.2	10.0	27.0	14.6	0.2	$Si_{1.0}B_{0.5}C_{1.3}N_{0.6}$

carbon species, the ratio of integrated intensity of the D band to that of the G band (I(D)/I(G)) measured in as-pyrolysed samples indicated that the samples display a similar (high) degree of disorder.

All samples contain also sp^2 boron nitride (BN) as reflected in the FTIR spectra (Fig. 2b) of the samples – in particular those with the lowest Si:B ratio (**SiBCN*3.75*_10** and **SiBCN*2.5*_10**) through the presence of the very broad bands in the wavenumber range 1470–1155 cm^{-1} and 1085-740 cm^{-1} which correspond to B–N stretching and B–N–B bending vibration modes, respectively [43]. The large band in the wavenumber range 1085–740 cm^{-1} most probably overlap bands attributed to Si–C and Si–N bonds.

These samples are X-ray amorphous as shown by the diffuse peaks identified in all the patterns (Fig. 2c) although the decrease of the Si:B ratio tends to reveal the (very) slow nucleation of the low temperature β-SiC (3C) polytype (ICDD PDF number: 00-029-1129) phases characterised by the large peaks at around 40° ((111) planes) and 70° ((311) planes). In addition, the patterns of the samples with the lowest Si:B ratio - from 5 to 2.5 - show a diffraction starting to emerge in the range of 25.8°–26.7° which could correspond to the (002) reflection of sp^2 C (graphite), BN (*h*-BN) and/or a mixed phase according to the fact that graphite and hexagonal boron nitride (*h*-BN) possess a hexagonal lattice structure with practically identical interlayer distances. Based on the increased content of BN with the decreased Si:B ratio and the fact that a rich variety of polymorphic C/BN heterostructures can be generated because of the ability to undergo homophilic (C–C) as well as heterophilic (C–B, C–N and B–N), this peak has been attributed to this mixed phase labeled B(C)N. Based on solid-state NMR we previously investigated [42], this B(C)N phase represents a mixture of BC_2N, BCN_2 and BN_3 units whose portion changes with the Si:B ratio. Thus, most probably, samples with high Si:B ratios (30 and 15) are made of an amorphous carbon-rich B(C)N phase whose (002) peak cannot be identified by XRD whereas low Si:B ratio (from 5 to 2.5) samples are composed of a turbostratic BN-rich B(C)N phase characterised by a (002) BN peak emerging in the XRD patterns of the corresponding samples. No additional phases have been detected in XRD patterns. Thus, the combination of X-ray diffraction and Raman/FTIR spectroscopies is in good agreement with the discussion made on elemental analyses and it highlights that Si–B–C–N ceramics obtained through the pyrolysis of boron-modified PSZ namely PSZB*X* ($2.5 \leq X \leq 30$) at 1000 °C in flowing nitrogen mainly display the signature of amorphous-Si_3N_4 and free carbon with a high degree of disorder for high Si:B ratios (low boron content) and the decrease of this parameter – the increase of the boron content - leads to the increased content of SiC and BN to the detriment of Si_3N_4 in the materials. SiC - and BN - nucleation occurred in as-pyrolysed samples with the lowest Si:B ratio. However, the corresponding peaks are too diffuse to measure a crystallite size with accuracy.

3.2. Thermal stability of as-pyrolysed boron-modified Si–C–N ceramics

The main interest of ceramics containing a homogeneous distribution of Si, B, C and N is the stability of their "disordered" long range structure against crystallization at very high temperature, especially compared to boron-free Si–C–N ceramics [39,40]. It was postulated that the turbostratic B(C)N phase identified above formed at high temperature shifts the carbothermal reaction of the Si_3N_4 phase composing Si-(B)–C–N ceramics toward higher temperatures by a kinetic stabilization mechanism [44]. Before discussing the crystallization evolution of the ceramics described in the present paper during their annealing step, we investigated their thermal stability, *i.e.*, **SiBCN*30*_10**, **SiBCN*15*_10**, **SiBCN*5*_10**, **SiBCN*3.75*_10** and **SiBCN*2.5*_10**, by high-temperature TG experiments up to 1800 °C in a nitrogen atmosphere (Fig. 2d). The measured weight changes have been discussed according to the elemental composition evolution of the same ceramics upon annealing. Thus, we followed the evolution in the Si, B, C and N contents of pristine powders - **SiBCN*15*_10, SiBCN*5*_10** and **SiBCN*2.5*_10** samples - through their heat-treatment in a nitrogen atmosphere at selected temperatures – 1400 (T = 14), 1600 (T = 16) and 1800 (T = 18) °C - with a dwelling time of 2 h at each temperature (Table 3). Annealed samples have been labeled **SiBCN*X*_T** with *X* corresponding to the Si:B molar ratio set for the preceramic polymer ($2.5 \leq X \leq 30$) and T ($14 \leq T \leq 18$) to the first two digits of the final annealing temperature as done with samples prepared at 1000 °C.

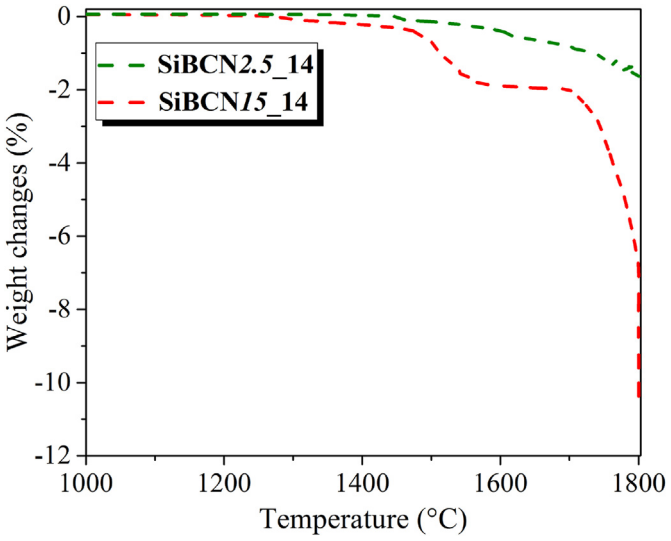

Fig. 3. TG curves of the **SiBCN*15*_14** and **SiBCN*2.5*_14** samples.

We can tentatively separate the TG curve evolutions into three temperature domains:

1) From 1000 to 1400 °C: a low weight loss continuously occurs most probably because powders prepared at 1000 °C still contain residual hydrogen (linked to Si and C) as demonstrated recently in the Si–B–C system [30]. Thus, the release of dihydrogen is probably the reason of the continuous low weight change observed in the temperature range 1000–1400 °C. This has been confirmed through the TG

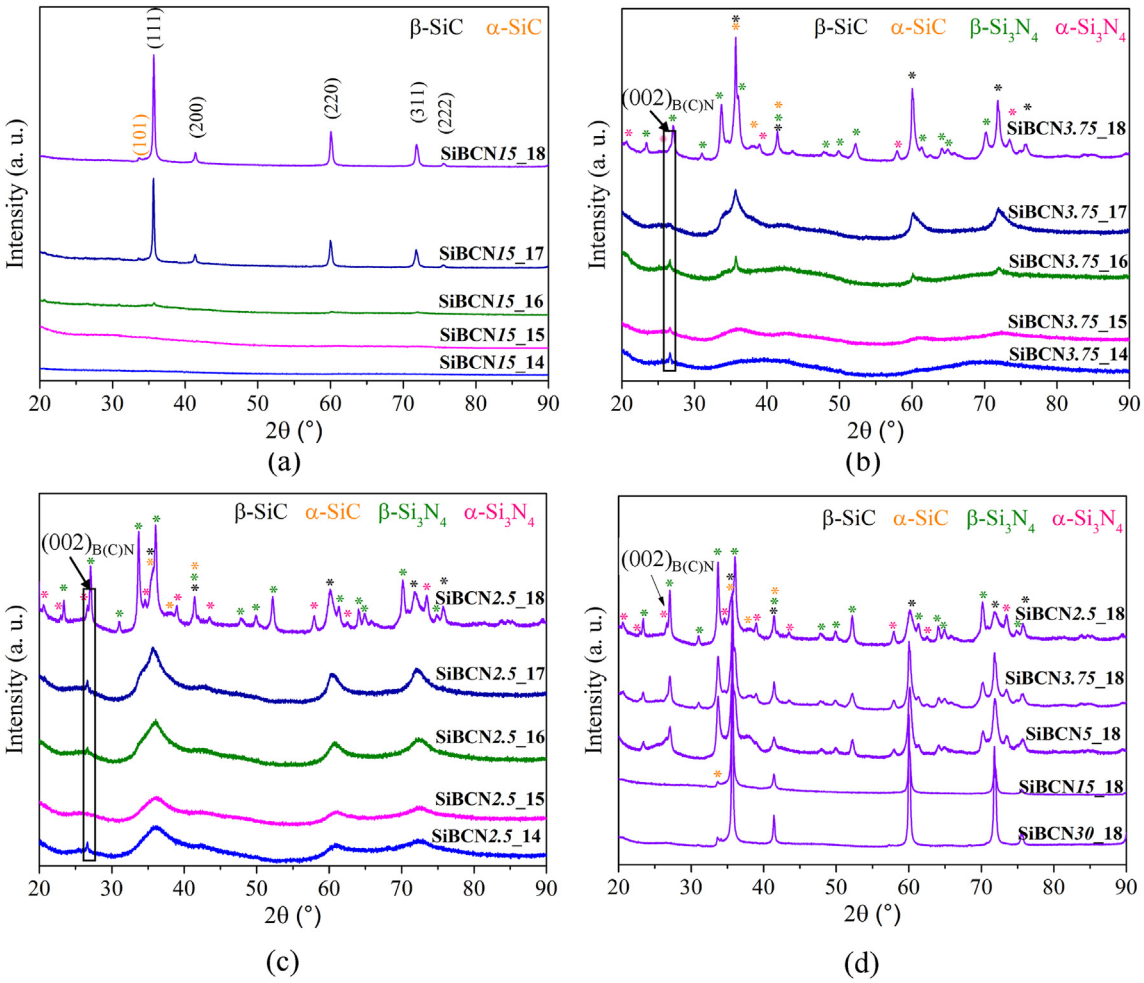

Fig. 4. Evolution of the XRD patterns of the **SiBCN*15*_10** (a) **SiBCN*3.75*_10** (b) and **SiBCN*2.5*_10** (c) samples in the temperature range 1400–1800 °C. XRD patterns of **SiBCN*X*_18** samples ($2.5 \leq X \leq 30$) (d).

investigations of the **SiBCN*15*_14** and **SiBCN*2.5*_14** samples (**SiBCN*15*_10** and **SiBCN*2.5*_10** samples annealed at 1400 °C for 2 h, Fig. 3) which did not show any weight loss.

2) In the 1400–1600 °C temperature range: the thermal behaviour of powders changed according to the Si:B ratios fixed at the polymer level. **SiBCN*30*_10** and **SiBCN*15*_10** samples exhibit an obvious and first weight loss of 3.52% and 1.74%, respectively. In contrast, the weight of the **SiBCN*5*_10**, **SiBCN*3.75*_10** and **SiBCN*2.5*_10** samples remains relatively stable (≈1% of weight loss). As generally discussed in Si–C–N and Si–B–C–N ceramics [31,36–40,45,46], this could point to the fact that a decomposition of amorphous-Si_3N_4 - as a major phase (68.5 $_{wt}$%) in samples with the highest Si:B ratio, i.e., **SiBCN*30*_10**, **SiBCN*15*_10** samples - started to occur in the presence of excess carbon leading to the formation of SiC and the release of nitrogen responsible of the weight loss identified by TG experiments. This reaction which occurs at a temperature above 1438 °C at a pressure of 1 atm of nitrogen [45,46] seems - however - to be limited between 1400 and 1600 °C according to the low observed weight loss of the considered samples and their elemental composition evolution reported in Table 3. Although the **SiBCN*15*_10** sample underwent a higher loss of nitrogen between 1400 °C (**SiBCN*15*_14**) and 1600 °C (**SiBCN*15*_16**) than the **SiBCN*5*_10** and **SiBCN*2.5*_10** samples annealed at the same temperatures (from **SiBCN*5*_14/SiBCN*2.5*_14** to **SiBCN*5*_16/SiBCN*2.5*_16**) for which the nitrogen content remained stable, these results indicated a smooth Si_3N_4 carbothermal reaction without sharp changes in the weight and N content of these samples with the highest Si:B ratio in the temperature range 1400–1600 °C.

3) In the temperature range 1600–1800 °C: the **SiBCN*30*_10** and **SiBCN*15*_10** samples undergo a second weight loss and lead to BN/SiC composites with a very low BN content and without free C based on the chemical formula of the **SiBCN*15*_18** sample indicated in Table 3. This result demonstrated the achievement of the carbothermal reaction (although the total weight loss measured at 1800 °C (around 15%) is relatively far from the weight loss measured for boron-free Si–C–N samples [39,40,45]) - and/or degradation into its elements - of Si_3N_4 in this temperature range although the decomposition of Si_3N_4 into liquid Si and N_2 is probably limited under nitrogen at this temperature [46,47]. In this temperature range, the weight loss of the **SiBCN*5*_10**, **SiBCN*3.75*_10** and **SiBCN*2.5*_10** samples proceeds at a higher rate at 1750 °C – with the most pronounced one for the **SiBCN*5*_10** sample. Based on the chemical formula of the **SiBCN*2.5*_18** sample, the nitrogen content – although decreasing - still remained high indicating the persistence of Si_3N_4 at 1800 °C in this sample. Thus, the **SiBCN*2.5*_10** sample which proposes the highest boron (9.0 $_{wt}$% (13.6 $_{at}$%))/BN (18.5 $_{wt}$%) contents in this series shows a relatively high stability and leads to a SiC/B(C)N/Si_3N_4 composite with a weight loss of 5.6% after annealing to 1800 °C. If stabilized at 1400 °C (**SiBCN*2.5*_14** sample), the weight loss is as low as 1.6% highlighting the high stability of this sample.

Based on these results, it seems that the evolutive composition of the B(C)N phase with the Si:B ratio - most probably associated with the

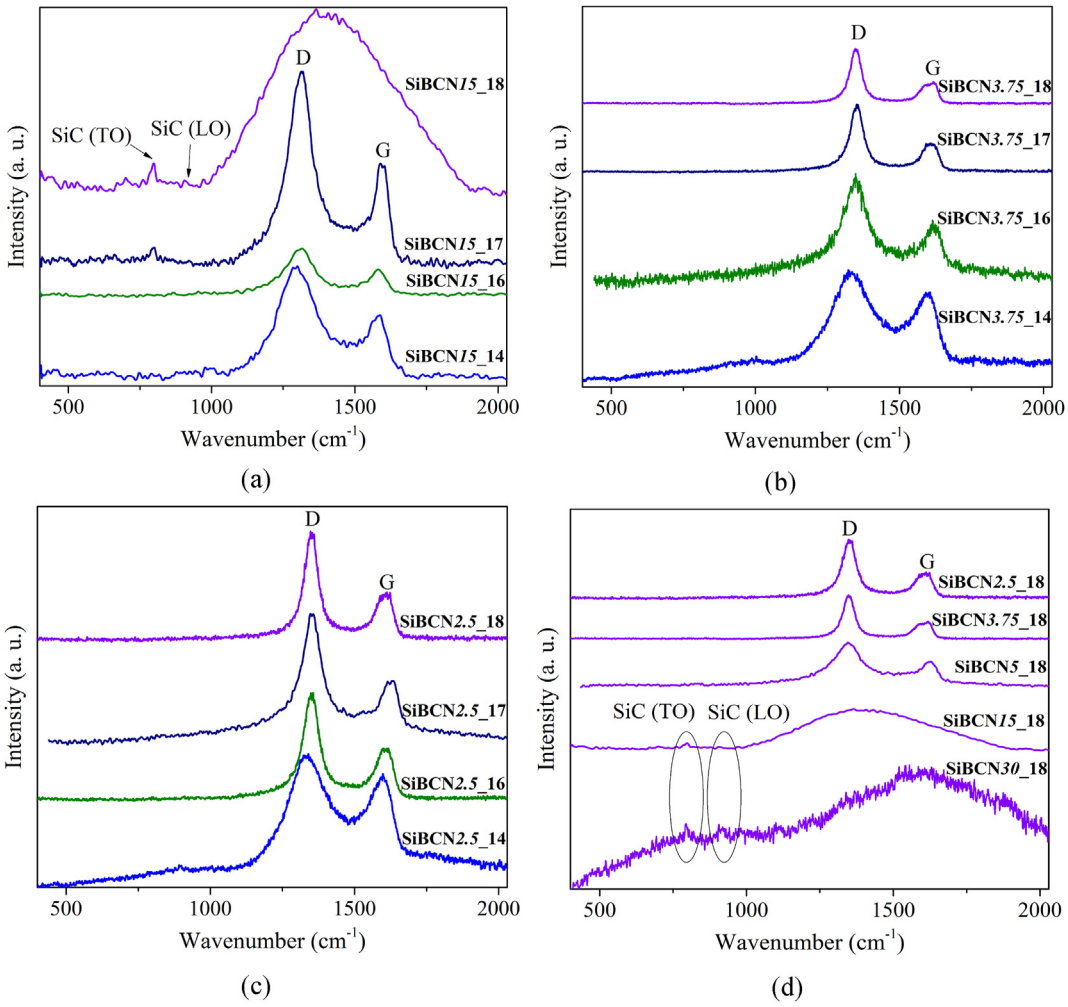

Fig. 5. Evolution of the Raman spectra of the **SiBCN*15*_10** (a) **SiBCN*3.75*_10** (b) and **SiBCN*2.5*_10** (c) samples in the temperature range 1400–1800 °C. Raman spectra of **SiBCN*X*_18** samples (2.5 ≤ X ≤ 30) (d).

decreased content of Si_3N_4 - modifies the thermal stability of Si–B–C–N ceramics. Indeed, the BN enrichment of this mixed phase with the decrease of the Si:B ratio clearly reduces and shifts to higher temperatures the weight loss of these ceramics upon annealing to 1800 °C; therefore, reducing the activity of sp^2-hybridised carbon toward the carbothermal reaction of amorphous-Si_3N_4. However, the temperature at which these samples start to decompose remains lower than the Si–B–C–N ceramics produced from boron-modified polysilazanes of the type $[B(SiRC_2H_4NH)_3]_n$ $[SiRC_2H_4NH]_{(x-3)n}$ (R = H, CH_3, $3 \leq x \leq 8$) that contain a maximum of 6.1 $_{wt}$% (≤9.5 $_{at}$%) of boron [36,39,40]; thereby a lower boron content than the samples investigated here. Thus, two more important prerequisites for obtaining high temperature stable Si–B–C–N materials are necessary: the amount of Si_3N_4 should not exceed a certain value while the SiC content should be high enough. As an illustration, the Si–B–C–N ceramics prepared from a boron-modified polysilazane of the type $[B(C_2H_4SiCH_3NH)_3]_n$ (C_2H_4 = CH_2CH_2, $CHCH_3$) and labeled T21 - containing Si_3N_4 and SiC phase contents of 20.1 wt% and 51.6 wt%, respectively - display one of the highest reported thermal stability among Si–B–C–N materials [36]. The Si_3N_4 (38.3 wt%) and SiC (27.4 wt%) phase contents of the most thermally stable **SiBCN*2.5*_10** sample (Table 2) - respectively 38 wt% and 29.2% for the **SiBCN*2.5*_14** sample - are relatively far from these values – despite the fact that the BN phase fraction is higher (18.8 and 19.2% for **SiBCN*2.5*_10** and **SiBCN*2.5*_14** samples, respectively). Thus, the large Si_3N_4:SiC phase content ratio seems to be the main reason of the lowest thermal stability of the samples developed in the present study. To complete our investigations and gain more information on the evolution of the chemical environment and bonding and the crystallization behaviour during the annealing of these ceramics at 1800 °C - mostly for samples with Si:B ratios of 15, 3.75 and 2.5 - a combination of technical experiments such as X-ray diffraction, Raman, solid-state NMR and FTIR spectroscopies and high-resolution TEM has been used.

3.3. *High-temperature phase and microstructure evolution in annealed boron-modified Si–C–N ceramics*

The structural evolution of these amorphous ceramics labeled **SiBCN*X*_10** (2.5 ≤ X ≤ 30) has been followed through the characterisation of annealed samples labeled **SiBCN*X*_T** (2.5 ≤ *X* ≤ 30, 14 ≤ T ≤ 18) at room temperature by X-ray diffraction (XRD, Fig. 4) and Raman spectroscopy (Fig. 5).

The broad and diffuse diffraction peaks in the XRD patterns of the **SiBCN*15*_14** (Fig. 4a) **SiBCN*3.75*_14** (Fig. 4b) and **SiBCN*2.5*_14** (Fig. 4c) samples indicate that the ceramics retain their global amorphous structure after annealing to 1400 °C although - as observed in as-pyrolysed samples (Fig. 2c) - the decrease of the Si:B ratio in samples annealed at 1400 °C involves the nucleation of the low temperature β-SiC (3C) polytype. The latter is characterised by the large peaks at 36.1, 61.1 and 72.6° which can be distinguished in the XRD pattern of the **SiBCN*2.5*_14** sample (Fig. 4c). From the (220) peak broadening, the SiC crystallite size in this sample is estimated to be around 2 nm. This is particularly evident when comparing with the XRD pattern of the

Table 4
Full width at half maximum (FWHM), 2θ diffraction angle, crystallite size (D_{SiC} and D_{Si3N4}) for SiC and Si_3N_4, lattice parameter (a) for SiC and Si_3N_4.

	β-SiC (220)				β-Si_3N_4 (200)			
Samples	FWHM (°)	2θ (°)	D_{SiC} (nm)	a (nm)	FWHM (°)	2θ (°)	D_{Si3N4} (nm)	a (nm)
SiBCN*30*_18	0.22	60.02	43.9	0.435	–	–	–	–
SiBCN*15*_18	0.21	60.15	43.9	0.435	–	–	–	–
SiBCN*5*_18	0.31	60.12	29.7	0.435	0.41	27.09	19.9	0.759
SiBCN*3.75*_18	0.33	60.04	28	0.435	0.37	27.07	22.1	0.759
SiBCN*2.5*_18	0.58	60.16	15.8	0.435	0.18	27.06	45.4	0.759

SiCN_14 sample which is flat in the same 2θ range (Fig. 1SIa, ESI) although zooms of the 20–40° and 60°–80° ranges tend to identify the presence of both α-Si_3N_4 and β-SiC phases (Fig. 1Sib and c, ESI). However, the nucleation process of SiC is clearly limited and a crystal size cannot be reached in boron-free samples. Thus, the gradual incorporation of boron in the early stage of the process from **PSZB*30*** to **PSZB*2.5*** promotes the crystallization of β-SiC in the derived ceramics annealed at 1400 °C. This observation supports the finding made by our group on the Si–B–C system [30] and by Tavakoli et al. on the Si–B–C–N system [38]. Concerning the α-Si_3N_4 phase identified in the XRD pattern of the **SiCN_14** sample (*See Fig. 1SIb in ESI)*, it could not be identified in the boron-containing samples. This tends to indicate that the incorporation of boron inhibits the nucleation of α-Si_3N_4. In addition, XRD patterns of the **SiBCN*3.75*_14** (Fig. 4b) and **SiBCN*2.5*_14** (Fig. 4c) samples display the diffraction (002) peak around 26.65° of the B(C)N phase indicating its enrichment in BN. A similar discussion can be provided after rising of the annealing temperature to 1500 °C, i.e., **SiBCN*15*_15** (Fig. 4a) **SiBCN*3.75*_15** (Fig. 4b) and **SiBCN*2.5*_15** (Fig. 4c) samples.

Clear changes occur between 1500 and 1600 °C - in particular for Si:B ratios of 15 and 3.75. XRD analyses show the appearance of sharper diffraction peaks in the XRD spectra of the **SiBCN*15*_16** (Fig. 4a and Fig. 2SI in ESI) and - to a much lower extent - **SiBCN*3.75*_16** (Fig. 4b) samples at positions attributable to the low temperature β-SiC (3C) polytype (35.74° (111), 60.19° (220) and 71.98° (311)) for both samples indicating the crystal growth of SiC. We measured SiC crystallite sizes of 35.9 nm for the **SiBCN*15*_16** sample and 19.2 nm for the **SiBCN*3.75*_16** sample. The main difference in the XRD patterns of the **SiBCN*15*_16** and **SiBCN*3.75*_16** samples is the persistence of the (002) peak of the B(C)N phase in the latter. This confirms the highest BN content of this phase in the **SiBCN*3.75*_16** sample. The very diffuse peaks centered at 36.1, 61.1 and 72.6° in the XRD patterns of the **SiBCN*2.5*_14** and **SiBCN*2.5*_15** samples are retained in the XRD pattern of the **SiBCN*2.5*_16** sample (Fig. 4c) at close positions. The SiC crystallite size of 2.3 nm shows that SiC crystal growth process is significantly reduced compared to the crystallization extent of SiC observed in the XRD pattern of the **SiBCN*15*_16** sample. The main peak centered at 36.1° has a shoulder on its left part at 33.7° which means that it is composed of several components which could be attributed to the (101) and (111) planes of the β-Si_3N_4 (ICDD PDF number: 04-033-1160) and β-SiC phases. Other major peaks at 60.8° (220), and 72.3° (311) can be attributed to β-SiC whereas the broad and poorly intense peak at 42.7° is attributable to the (201) planes of β-Si_3N_4. The XRD reflections are too broad, however, to permit analysis of the peak shapes or to accurately determine the lattice parameters of the β-Si_3N_4 phase indicating that Si_3N_4 nucleation is limited at this temperature. As observed in the **SiBCN*3.75*_16** sample, we still identify the (002) peak of the BN-rich B(C)N phase in the **SiBCN*2.5*_16** sample.

Whereas the **SiBCN*15*_17** (Fig. 4c) sample can be considered as a pure SiC with a crystallite size of 39.5 nm based on the presence of the main XRD peaks of β-SiC ((111), (200), (220), (311) and (222)), the decrease of the Si:B ratio tends to limit the crystallization process of SiC as attested in the XRD patterns of the **SiBCN*3.75*_17** and **SiBCN*2.5*_17** samples. Furthermore, the presence of the peak corresponding to the (101) planes of β-Si_3N_4 (33.7°) in the patterns of both samples marks the initiation of the β-Si_3N_4 nucleation in these samples (Fig. 4b and c).

After annealing at 1800 °C, all analyzed samples display XRD patterns characteristic of crystallized ceramics (Fig. 4a–c). Fig. 4d highlights the high temperature phase evolution in **SiBCN*X*_18** samples according to their Si:B (X) ratio ($2.5 \leq X \leq 30$). Thus, the decrease of the Si:B ratio tends to complexify the XRD patterns of those samples while reducing the peak intensity. The crystallization process is completed at 1800 °C in samples with high Si:B ratios which display the signature of a single crystalline phase, i.e., SiC with the β phase as a major phase, whereas those with a low Si:B ratio can be considered as composite materials composed of the B(C)N phase - the corresponding peak overlaps the peak attributed to Si_3N_4 - as well as the α and β phases of SiC and Si_3N_4. The presence of hexagonal polytypes of α-SiC (6H–SiC, ICDD PDF number: 00-029-1131) - identified by additional peaks emerging at 34.08° for plane (101) and at 38.3° for plane (103) in the **SiBCN*3.75*_18** and **SiBCN*2.5*_18** samples - could be related to a β-to α- SiC transformation [48] and in particular to the creation of stacking faults that act as nuclei for these unstable polytypes during the preferred β-SiC crystallization. In addition, we can identify the peaks attributed to the α-Si_3N_4 phase (ICDD PDF number: 04-005-5074) in the XRD patterns of the **SiBCN*3.75*_18** and **SiBCN*2.5*_18** samples which could result from a β-to α-transformation as observed during the sintering procedure of amorphous Si_3N_4 [49].

A semi-quantitative estimation of the extent of crystallization has been achieved by calculating the integrated intensity of the Gaussian curve fitting of the (220) diffraction peak from β-SiC and (200) from β-Si_3N_4 lines. Peak positions have been measured and crystallite sizes have been calculated from the FWHM of the above diffraction lines using the Scherrer formula (Table 4). The obtained results gathered in Table 4 show that the estimated average crystallite size of β-SiC is affected by the ceramic's boron content.

Interestingly, we previously concluded that the gradual incorporation of boron in the early stage of the process increased the tendency of β-SiC crystallization in as-pyrolysed Si–B–C–N ceramic powders (1000 °C) and those annealed at 1400 °C (See XRD patterns of the **SiBCN*15*_14** (Fig. 4a) **SiBCN*3.75*_14** (Fig. 4b) and **SiBCN*2.5*_14** (Fig. 4c) samples). After annealing at 1800 °C, it can be seen that SiC crystal growth – directly related to the peak linewidth – is limited in samples with a high boron content, i.e. low Si:B ratio; most probably because of the limited occurrence of the carbothermal reaction of amorphous Si_3N_4 due to the formation of a BN-rich B(C)N phase that tends to modify the activity of sp^2-hybridised carbon in such materials. In addition, the lattice parameter of cubic SiC has also been calculated. We can observe that the lattice parameter of β-SiC is not affected by the boron content in the samples. Considering that an increase of the lattice parameter of β-SiC is due to boron incorporation into the β-SiC phase [50] whereas its reduction is associated with the formation of a SiC/C solid solution [51], this confirms that no boron is incorporated into the β-SiC lattice in our samples. As mentioned earlier, Si_3N_4 crystal growth proceeds at 1800 °C in high B content samples as indicated through the highest crystallite size calculated in the **SiBCN*2.5*_18** sample. By considering the fact that the conversion of a-Si_3N_4 into β-SiC relies – in part - on the activity of the sp^2-hybridised C in the B(C)N phase, we tended to gain more information about this mixed phase by focusing on the (002) peak at around 26.65° we attributed to the B(C)N phase (See Fig. 4b, c and d). In the present paper, there is no evidence of a gradual shift of this (002) diffraction peak

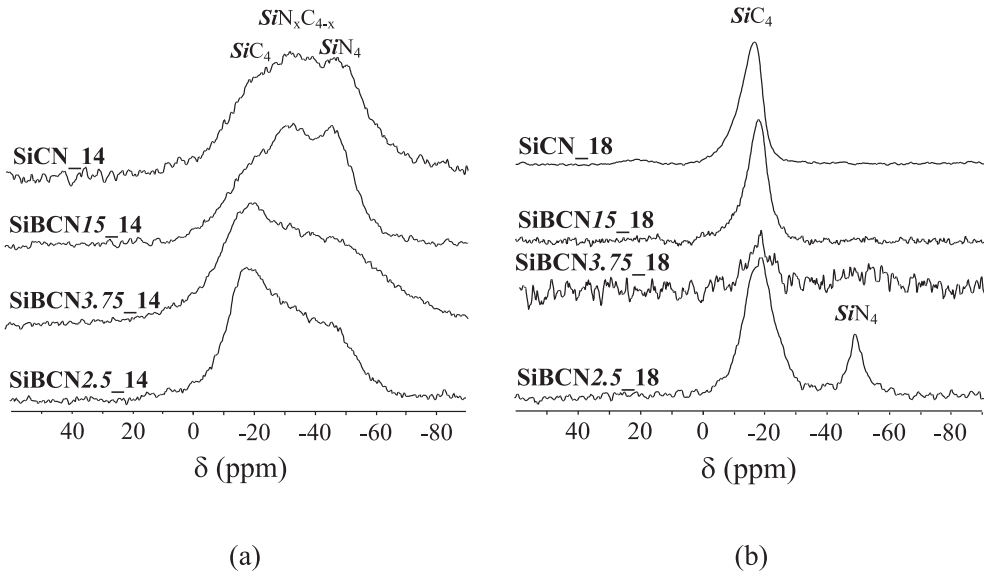

Fig. 6. Experimental ^{29}Si MAS NMR for the **SiCN_14**, **SiBCN*15*_14**, **SiBCN*3.75*_14** and **SiBCN*2.5*_14** samples (a) and **SiCN_18**, **SiBCN*15*_18**, **SiBCN*3.75*_18** and **SiBCN*2.5*_18** samples (b) recorded at 7 T.

with both the annealing temperature and the Si:B ratio. Thus, this demonstrates that the interlayer spacing, i.e., d_{002}, does not evolve with such parameters. This is due to the fact that graphite and hexagonal boron nitride (h-BN) possess a hexagonal lattice structure with practically identical interlayer distances because of the similarity in the overall binding energy curves of both materials [52]. Thus, it is clear that the C, B and N content of this B(C)N phase changes with the decrease of the Si:B ratio in samples. As previously discussed, it represents a carbon-rich mixed phase for high Si:B ratios (low B content) with a strong activity toward the carbothermal reaction of amorphous-Si_3N_4 and a BN-rich mixed phase for low Si:B ratios (high B content) significantly decreasing the carbon activity. Thus, the persistence of this peak (Fig. 4d) with the decrease of the Si:B ratio means that this B(C)N phase enriches with BN with the decrease of the Si:B ratio in samples.

Raman spectroscopy (Fig. 5) is one of the most sensitive techniques to characterise the disorder in sp^2 carbon materials. The spectra of samples annealed at 1400 °C, i.e., **SiBCN*15*_14** (Fig. 5a) **SiBCN*3.75*_14** (Fig. 5b) and **SiBCN*2.5*_14** (Fig. 5c) samples, exhibit very distinct and narrow bands of the defect-induced D (originates from the breathing mode A_{1g} of the sp^2 rings) and graphitic G bands (arises from the stretching mode E_{2g} of the sp^2 C–C bonds) at ~1355 cm^{-1} and ~1590 cm^{-1}, respectively.

If we consider low boron content samples (**SiBCN*15*_X**, Fig. 5a), we observe the progressive disappearance of those two carbon bands after annealing at 1800 °C (**SiBCN*15*_18**), concomitant with the appearance of a peak around 800 cm^{-1} assigned to SiC. This confirms the presence of a carbon-rich B(C)N phase that involved the carbothermal reaction of amorphous Si_3N_4. However, although the amount of boron introduced was not enough to prevent the carbothermal reaction of amorphous Si_3N_4, it was still enough to push back the temperature of this reaction in comparison to the observation made for boron-free materials derived from PSZ (Fig. 3SI in ESI). Indeed, a transition is observed between the **SiCN_15** sample which presents carbon bands in its Raman spectrum and the **SiCN_16** sample which exhibits only bands related to the two vibrational modes of SiC in its spectrum. Thus, a shift of 200 °C occurs in the **SiBCN*15*_T** sample. The decrease of the Si:B ratio (**SiBCN*3.75*_T** (Fig. 5b) and **SiBCN*2.5*_T** (Fig. 5c)) allowed retaining the carbon bands on the whole annealing temperature range from 1400 to 1800 °C which confirms that the activity of sp^2-hybridised C is reduced because of the formation of a BN-rich B(C)N phase. This is clear in Fig. 5d which compares samples annealed to 1800 °C according to their Si:B ratio: carbon bands gradually appeared while bands attributable to SiC disappeared with the decrease of the Si:B ratio. The ratio of integrated intensity of the D band to that of the G band (I(D)/I(G)) measured in samples annealed at 1800 °C indicated that the degree of disorder remains quite stable with the change of the Si:B ratio. It is important to mention that no bands related to Si_3N_4 could be identified in samples with the lowest Si:B ratio. In addition, we could not identify the signature of BN because the D and G bands of graphite overlap the band of h-BN appearing around 1360 cm^{-1} [53].

3.4. Chemical environment and bond evolution in the ceramics at high temperature

The evolution of the chemical environments around silicon and boron of these amorphous ceramics has been followed by solid-state NMR through the characterisation of the **SiBCN*15*_10**, **SiBCN*3.75*_10** and **SiBCN*2.5*_10** samples - consisting of SiN_xC_{4-x} ($0 \leq x \leq 4$) type units with boron mainly involved in BCN_2/BN_3 units [42] – after annealing at 1400 °C (**SiBCN*15*_14**, **SiBCN*3.75*_14** and **SiBCN*2.5*_14** samples, Fig. 6a) and 1800 °C (**SiBCN*15*_18**, **SiBCN*3.75*_18** and **SiBCN*2.5*_18** samples, Fig. 6b). NMR spectra have been compared to those of the boron-free SiCN samples at the same annealing temperature (**SiCN_14** and **SiCN_18**).

Solid-state NMR data highlight results gained from elemental analyses. An annealing treatment at 1400 °C (**SiBCN*15*_14**, **SiBCN*3.75*_14** and **SiBCN*2.5*_14** samples, Fig. 6a) does not induce significant changes in the chemical environment of Si (compared to as-pyrolysed powders [42]) as attested by the identification of a broad signal attributed to **Si**N_xC_{4-x} ($0 \leq x \leq 4$) environments. More precisely, this signal can be deconvoluted in three main components: one around −18 ppm (typical of **Si**C_4 environments in SiC), one around – 31 ppm (assigned to **Si**N_xC_{4-x} ($2 \leq x \leq 3$ mixed units) and the last one around −45 ppm (attributed to **Si**N_4 units in Si_3N_4). By comparison to the boron-free ceramics derived from PSZ labeled **SiCN_14**, we can see that the proportion of mixed **Si**N_xC_{4-x} ($2 \leq x \leq 3$) units tends to increase compared to non-mixed **Si**C_4 and/or **Si**N_4 environments with decreasing Si:B ratio. Moreover, the signal intensity of SiC_4 environments increases to the detriment of SiN_4 environments with decreasing Si:B ratio, in good agreement with elemental analyses that demonstrated an increase of the SiC content to the detriment of Si_3N_4 in the ceramics. Cardurner et al. showed the importance of stacking faults in β-SiC samples: they found that the ^{29}Si NMR response could be either a narrow peak around −16 ppm for an ordered β phase as a

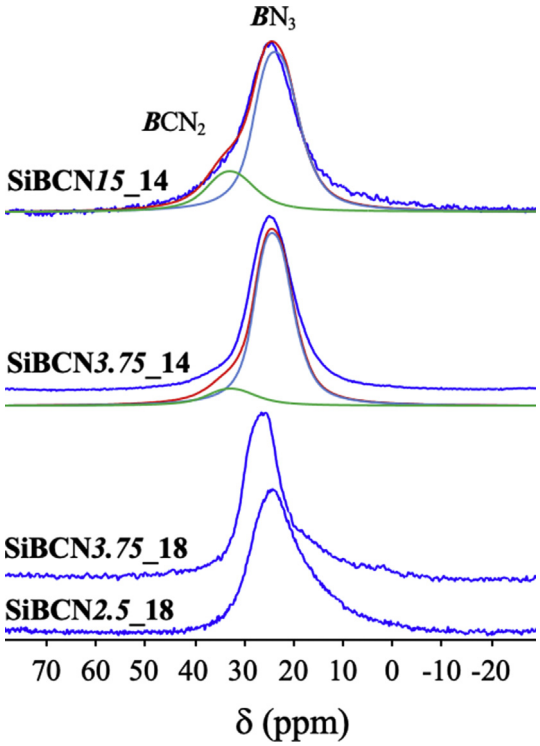

Fig. 7. ^{11}B MAS NMR experimental and simulated spectra recorded at 16.4 T for the **SiBCN*15*_14**, **SiBCN*3.75*_14**, **SiBCN*3.75*_18** and **SiBCN*2.5*_18** samples.

predominant component, accompanied by some minor features due to structure units of α-phases, or a broader signal centered at −18/-19 ppm related to a disordered structure [48]. They concluded that these differences came from the formation of stacking disorders in the SiC particles. As a consequence, we can confirm the poor crystallization of the β-SiC phase after annealing to 1400 °C. After annealing at 1800 °C (**SiBCN*15*_18**, **SiBCN*3.75*_18** and **SiBCN*2.5*_18** samples, Fig. 6b), all spectra show **Si**C_4 environments characterised by a sharper signal at around −18 ppm related to an ordering of the various Si sites in a more crystalline structure. Such a NMR response is expected for the **SiBCN*15*_18** sample because of the formation of SiC due to the carbothermal reaction of amorphous Si_3N_4. The signal related to **Si**N_4 units tends to emerge in the spectrum of the **SiBCN*3.75*_18** sample and is clearly visible in the spectrum of the **SiBCN*2.5*_18** sample. The corresponding signal is most probably made of several components according to the formation of the α- and β-phases of Si_3N_4 [54]. Therefore, we can confirm the relatively good stability of the Si_3N_4 phase in presence of a high boron content in Si–B–C–N samples. The NMR spectrum of the **SiBCN*2.5*_18** sample display the broadest **Si**C_4 signal indicating the presence of a disordered β-SiC phase, but also the presence of Si sites characteristic of structure units of α-polytypes [48] as a confirmation of XRD results. Experimental ^{11}B MAS NMR spectra recorded at 16.3 T are shown in Fig. 7.

^{11}B MAS NMR spectra of the **SiBCN*15*_14** and **SiBCN*3.75*_14** samples exhibit a main broad resonance centered in the region of tri-coordinated boron atoms (B [3]) that can be tentatively simulated with two sites suggesting a distribution of **B**CN_2 and **B**N_3 units [55–61]. The contribution of **B**CN_2 units decreases with decreasing Si:B ratio and they even disappear after annealing at 1800 °C to form only **B**N_3 units for the lowest Si:B ratios. These observations are highly consistent with the FT-IR spectroscopy studies on annealed samples (Fig. 8). In particular, the spectra recorded for the **SiBCN*15*_14**, **SiBCN*3.75*_14** and **SiBCN*2.5*_14** samples contain broad and overlapped - especially for high Si:B ratios - signals still indicating a variety of elemental bonds including Si–C, Si–N and B–N with a lack of long-range order. They evolve towards narrower

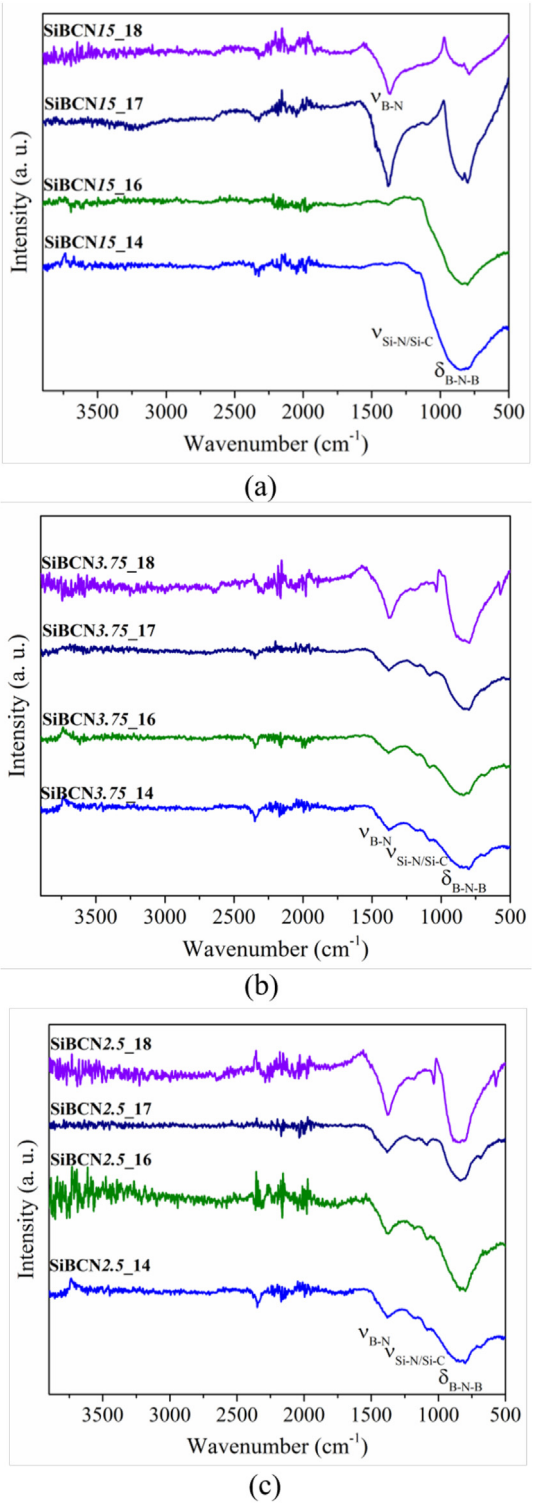

Fig. 8. FTIR spectra of the **SiBCN*15*_10**, **SiBCN*3.75*_10** and **SiBCN*2.5*_10** samples annealed in the temperature range 1400–1800 °C.

and separated signals in the spectra recorded for the **SiBCN*15*_18**, **SiBCN*3.75*_18** and **SiBCN*2.5*_18** samples because of the development of well-organized phases containing B–N bonds of sp^2 type (B–N stretching around 1380 cm^{-1} and B–N–B bending around 800 cm^{-1}) associated to a phase similar to h-BN [43]. Interestingly, two more absorption bands can be noticed at 571 cm^{-1} and 1036 cm^{-1} in the spectra of **SiBCN*3.75*_18** and **SiBCN*2.5*_18** samples. They are characteristic of the presence of β-Si_3N_4 crystalline phases [62] as suggested by solid-state ^{29}Si NMR.

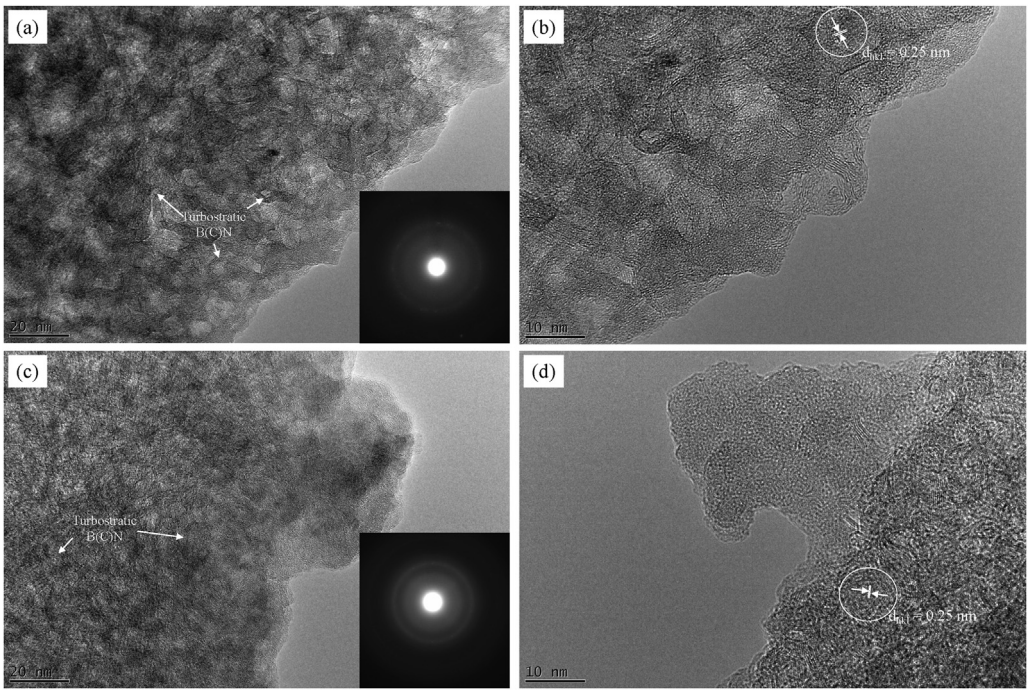

Fig. 9. High-resolution TEM images and corresponding SAED patterns of the **SiBCN*30*_14** (a, b) and **SiBCN*2.5*_14** (c, d) samples.

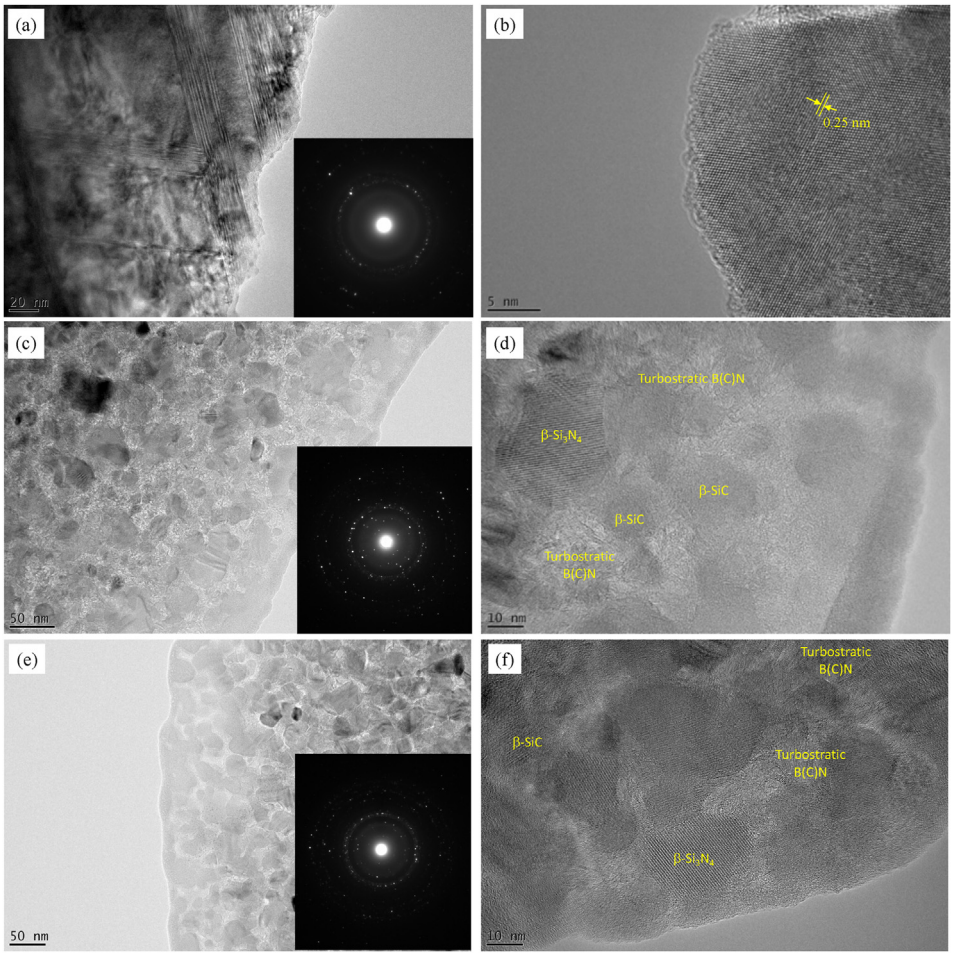

Fig. 10. High-resolution TEM images and corresponding SAED patterns of the **SiBCN*30*_18** (a, b), **SiBCN*5*_18** (c, d) and **SiBCN*2.5*_18** (e, f) samples.

Thus, they confirm the long-range organization of Si_3N_4 in Si–B–C–N samples with a high boron content.

3.5. Local structural rearrangements of Si–B–C–N ceramics during annealing

To assess the micro-/nanostructure of Si–B–C–N ceramics derived from boron-modified PSZ, the **SiBCN*30*_14**, **SiBCN*2.5*_14**, **SiBCN*30*_18**, **SiBCN*5*_18** and **SiBCN*2.5*_18** samples have been further studied by means of high-resolution TEM (Figs. 9–10).

Fig. 9a reports the low magnification TEM image of the **SiBCN*30*_14** sample which consists of a majority of zones with graphene-like carbon ribbons and minor domains consisting of turbostratic carbon. The associated SAED pattern, showing very small spot identifying the β-SiC phase in the material, shows that – although the boron content in the materials is low – SiC nucleation already started in such a material (See Fig. 2SI in ESI). As a result, the higher magnification image in Fig. 9b highlights the nucleation of SiC with a fringe spacing of 0.25 nm corresponding to the d-spacing of the lattice plane of the β-SiC structure, i.e. the (111) direction, embedded in a matrix of the carbon-rich B(C)N phase.

Same comments can be made on the TEM image of the **SiBCN*2.5*_14** sample: it mainly consists of layered areas as shown in Fig. 9c which surround very small SiC nuclei (Fig. 9d) highlighting XRD observations. TEM image and SAED pattern observations of the samples annealed at 1800 °C, i.e., **SiBCN*30*_18**, **SiBCN*5*_18** and **SiBCN*2.5*_18** samples (Fig. 10), are in good agreement with the fact that such samples represent crystalline ceramics as previously discussed through XRD, Raman, NMR and FTIR spectroscopies. The TEM image and SAED pattern observations of the **SiBCN*30*_18** sample (Fig. 10 a, b) indicated a relatively high degree of crystallization with numerous stacking faults most probably created during the rapid SiC crystal growth (Fig. 10a) and distinct spots which can be indexed to some planes of the β-SiC phase (Fig. 10b). In Fig. 4SI in ESI, we can observe fringe systems which are characteristic of stacking faults or twins in the picture and the interplanar spacings - determined based on the distance from the reflection to the pattern center - confirm that the experimental data on interplanar distances are close to the theoretical ones for the β-SiC cubic lattice. In particular they correspond to the (111), (200), (220), (311), (331) and (511) planes. The contrast variations in the bright field TEM micrographs in Fig 10 c to f show that a phase segregation occurred after annealing at 1800 °C in the **SiBCN*5*_18** and **SiBCN*2.5*_18** samples. **SiBCN*5*_18** and **SiBCN*2.5*_18** specimens consist of homogeneously dispersed relatively small SiC and Si_3N_4 nuclei (dark contrast) - the presence of β-Si_3N_4 and β-SiC has been confirmed through the investigation of the SAED patterns - and turbostratic B(C)N embedded in a network with the typical phase contrast of a poorly crystallized matrix. Lattice fringes of the nanocrystals – with diameter less than 50 nm - confirm that the samples represent nanocomposites with a fringe spacing of 0.66 nm and 0.25 nm corresponding to the d-spacing of the lattice plane of the β-Si_3N_4 and β-SiC structure, i.e. the (100) and (111) directions, in the **SiBCN*5*_18** (Fig. 10c and d) and **SiBCN*2.5*_18** (Fig. 10e and f) samples. It was not possible to identify the α-phases of SiC and Si_3N_4. Thus, annealing at 1800 °C of high boron content samples provides access to composites composed of SiC, Si_3N_4 and a BN-rich B(C)N phase content.

4. Conclusion

We investigated the thermal stability, phase evolution and crystallization in Si–B–C–N ceramics derived from a poly (vinylmethyl-co-methyl)silazane (Durazane® 1800 by Merck) modified with various amounts of borane dimethylsulfide (BDMS). Using several and complementary characterisation tools such as elemental analysis, XRD, HT-TGA, FTIR, Raman and solid-state NMR spectroscopies and HR-TEM, we followed the thermal and structural behaviour evolution of a series of amorphous Si–B–C–N ceramics formed at 1000 °C during their annealing from 1400 to 1800 °C. We showed that we could control the boron content of these ceramics in the early stage of the process – at the polymer level – to produce samples that demonstrated tailored amorphous-to-crystalline transition. The boron content has a clear effect on the thermal stability of the amorphous SiN_xC_{4-x} ($0 \leq x \leq 4$) phase in the various ceramics during their annealing to 1800 °C. Boron modification of the Si–C–N ceramics tends to form a B(C)N phase whose composition evolves with the change of the Si:B ratio affecting the carbothermal reaction of amorphous Si_3N_4. A boron content of 13.6 wt% (i.e., 18.8 wt% of BN) allowed to produce highly stable Si–B–C–N ceramics although this stability by the excess Si_3N_4:SiC phase content ratio. Thus, the thermal stability of these amorphous ceramics is intimately linked to the phase content generated in amorphous ceramics after pyrolysis at 1000 °C. Low boron content Si–B–C–N ceramics – fully amorphous after pyrolysis to 1000 °C and annealing to 1400 °C- evolve toward pure β-SiC most probably surrounding a small portion of BN nuclei after annealing to 1800 °C. In high boron content Si–B–C–N ceramics, the nucleation of nanosized β-SiC takes place in as-pyrolysed samples and those formed after annealing at 1400 °C/2 h to the detriment of the crystallization of α-Si_3N_4. However, SiC crystal growth was very limited upon annealing at 1800 °C; especially because of the formation of a BN-rich B(C)N phase we could assimilate to a C/BN heterostructure that reduces the activity of sp^2-hybridised C toward the carbothermal reaction of amorphous-Si_3N_4 in such samples. Thus, high boron content Si–B–C–N ceramics display a microstructure composed of SiC and Si_3N_4 crystallites, surrounded by ribbons of a turbostratic BN-rich B(C)N phase in an amorphous matrix after annealing at 1800 °C.

Declaration of competing interest

The authors declare that they have no known competing financial interests or personal relationships that could have appeared to influence the work reported in this paper.

Acknowledgment

SB and GC would like to gratefully acknowledge the financial contribution from Région Nouvelle-Aquitaine (post-doc fellows of Dr. Marion Schmidt and Dr. Mélanie Wynn). SB, GC and FR would like to thank ANRT for its financial support of the PhD theses of Marion Schmidt and Diane Fonblanc. SB would like to thank the funding agency Agence Nationale de la Recherche (ANR) for supporting this work through the Polyceramem project (Project number ANR-13-BS08-009, PhD thesis of Dr. Antoine Viard) and the Carbofibers project (Projet number ANR-15-CE09-0022, PhD thesis of Dr. David Lopez-Ferber). The French Région Ile de France - SESAME program is acknowledged for financial support (700 MHz spectrometer).

Appendix A. Supplementary data

Supplementary data to this article can be found online at https://doi.org/10.1016/j.oceram.2021.100055.

References

[1] H.P. Baldus, M. Jansen, Novel high-performance ceramics-amorphous inorganic networks, from molecular precursors, Angew. Chem. Int. Ed. 36 (1991) 328–343.
[2] D.R. Ulrich, in: R.M. Laine (Ed.), Better Ceramics through Chemistry in Transformation of Organometallics into Common and Exotic Materials: Design and Activation, Martinus Nijhoff Publishers, 1988, pp. 207–235.
[3] M. Peuckert, T. Vaahs, M. Bruck, Ceramics from organometallic polymers, Adv. Mater. 2 (1990) 398–404.
[4] J. Bill, F. Aldinger, Precursor-derived covalent ceramics, Adv. Mater. 7 (1995) 775–787.
[5] P. Greil, Polymer derived engineering ceramics, Adv. Eng. Mater. 2 (2000) 339–348.
[6] P. Colombo, G.D. Soraru, R. Riedel, H.-J. Kleebe, Polymer Derived Ceramics: from Nano-Structure to Applications, DEStech Publications, Lancaster, 2009.

[7] P. Colombo, G. Mera, R. Riedel, G.D. Soraru, Polymer-derived ceramics: 40 years of research and innovation in advanced ceramics, J. Am. Ceram. Soc. 93 (2010) 1805–1837.
[8] S. Bernard, Design, Processing, and Properties of Ceramic Materials from Preceramic Precursors, Nova Science Pub Inc., 2012.
[9] G. Mera, M. Gallei, S. Bernard, E. Ionescu, Ceramic nanocomposites from tailor-made preceramic polymers, Nanocomposites 5 (2015) 468–540.
[10] E. Ionescu, H.-J. Kleebe, R. Riedel, Silicon-containing polymer-derived ceramic nanocomposites (PDC-NCs): preparative approaches and properties, Chem. Soc. Rev. 41 (2012) 5032–5052.
[11] M. Zaheer, T. Schmalz, G. Motz, R. Kempe, Polymer derived non-oxide ceramics modified with late transition metals, Chem. Soc. Rev. 41 (2012) 5102–5116.
[12] C. Stabler, E. Ionescu, M. Graczyk-Zajac, I. Gonzalo-Juan, R. Riedel, Silicon oxycarbide glasses and glass-ceramics: "All-Rounder" materials for advanced structural and functional applications, J. Am. Ceram. Soc. 101 (2018) 4817–4856.
[13] A. Viard, D. Fonblanc, D. Lopez-Ferber, M. Schmidt, A. Lale, C. Durif, M. Balestrat, F. Rossignol, M. Weinmann, R. Riedel, S. Bernard, Polymer derived Si-B-C-N ceramics: 30 years of research, Adv. Eng. Mater. 20 (2018) 1800360–1800371.
[14] E. Ionescu, S. Bernard, R. Lucas, P. Kroll, S. Ushakov, A. Navrotsky, R. Riedel, Ultrahigh temperature ceramics (UHTCs) and related materials – syntheses from polymeric precursors and energetics, Adv. Eng. Mater. 21 (2019) 1900269–1900292.
[15] Q. Wen, Z. Yu, R. Riedel, The fate and role of in situ formed carbon in polymer-derived ceramics, Prog. Mater. Sci. 109 (2020) 100623–100685.
[16] S. Bernard, C. Salameh, P. Miele, Boron nitride ceramics from molecular precursor: synthesis, properties and applications, Dalton Trans. 45 (2016) 861–873.
[17] A. Lale, M. Schmidt, M.D. Mallmann, A.V.A. Bezerra, E. Diz Acosta, R.A.F. Machado, U.B. Demirci, S. Bernard, Polymer-derived ceramics with engineered mesoporosity: from design to application in catalysis, Surf. Coating. Technol. 350 (2018) 569–586.
[18] C. Vakifahmetoglu, D. Zeydanli, P. Colombo, Porous polymer derived ceramics, Mater. Sci. Eng. R 106 (2016) 1–30.
[19] A. Viard, P. Miele, S. Bernard, Polymer-derived ceramics route toward SiCN and SiBCN fibers: from chemistry of polycarbosilazanes to the design and characterisation of ceramic fibers, J. Ceram. Soc. Jpn. 124 (2016) 967–980.
[20] O. Flores, R.K. Bordia, D. Nestler, W. Krenkel, G. Motz, Ceramic fibers based on SiC and SiCN systems: current research, development, and commercial status, Adv. Eng. Mater. 16 (2014) 621–636.
[21] G. Barroso, Q. Li, R.K. Bordia, G. Motz, Polymeric and ceramic silicon-based coatings – a review, J. Mater. Chem. 7 (2019) 1936–1963.
[22] D. Hotza, R. Nishihora, R. Machado, P.-M. Geffroy, T. Chartier, S. Bernard, Tape casting of preceramic polymers towards advanced ceramics: a review, Int. J. Ceramic Eng. Sci. 1 (2019) 21–41.
[23] S. Ishihara, H. Gu, J. Bill, F. Aldinger, F. Wakai, Densification of precursor-derived Si-C-N ceramics by high-pressure hot isostatic pressing, J. Am. Ceram. Soc. 85 (2002) 1706–1712.
[24] M.J. Gasch, J. Wan, A.K. Mukherjee, Preparation of a Si_3N_4/SiC nanocomposite by high-pressure sintering of polymer precursor derived powders, Scripta Mater. 45 (2001) 1063–1068.
[25] O. Majoulet, M.C. Bechelany, F. Sandra, G. Bonnefont, G. Fantozzi, L. Joly-Pottuz, A. Malchere, S. Bernard, P. Miele, Silicon-boron-carbon-nitrogen monoliths with high, interconnected and hierarchical porosity, J. Mater. Chem. 1 (2013) 10991–11000.
[26] M.C. Bechelany, C. Salameh, A. Viard, L. Guichaoua, F. Rossignol, T. Chartier, S. Bernard, P. Miele, Preparation of polymer-derived Si-B-C-N monoliths by spark plasma sintering technique, J. Eur. Ceram. Soc. 35 (2015) 1361–1374.
[27] S. Bernard, P. Miele, Ordered mesoporous polymer-derived ceramics and their processing into hierarchically porous boron nitride and SilicoBoron CarboNitride monoliths, New J. Chem. 38 (2014) 1923–1931.
[28] J. Yuan, D. Li, K.E. Johanns, C. Fasel, K. Durst, H.-J. Kleebe, Z. Shen, R. Riedel, E. Ionescu, Preparation of dense SiHf(B)CN-based ceramic nanocomposites via rapid spark plasma sintering, J. Eur. Ceram. Soc. 37 (2017) 5157–5165.
[29] A. Rahman, A. Singh, S.P. Harimkar, R.P. Singh, Mechanical characterisation of fine-grained silicon carbide consolidated using polymer pyrolysis and spark plasma sintering, Ceram. Int. 40 (2014) 12081–12091.
[30] M. Balestrat, E. Diz Acosta, O. Hanzel, N. Tessier-Doyen, R. Machado, P. Šajgalík, Z. Lenčéš, S. Bernard, Additive-free low temperature sintering of amorphous Si-B-C powders derived from boron-modified polycarbosilanes: toward the design of SiC with tunable mechanical, electrical and thermal properties, J. Eur. Ceram. Soc. 40 (2020) 2604–2612.
[31] R. Riedel, A. Kienzle, W. Dressler, L. Ruwisch, J. Bill, F. Aldinger, Nature 382 (1996) 796–798.
[32] P. Baldus, M. Jansen, D. Sporn, Ceramic fibers for matrix composites in high-temperature engine applications, Science 285 (1999) 699–703.
[33] D. Fonblanc, D. Lopez-Ferber, M. Wynn, A. Lale, A. Soleilhavoup, A. Leriche, Y. Iwamoto, F. Rossignol, C. Gervais, S. Bernard, Crosslinking chemistry of poly(vinylmethyl-co-methyl)silazanes toward low-temperature formable preceramic polymers as precursors of functional aluminium-modified Si-C-N ceramics, Dalton Trans. 47 (2018) 14580–14593.
[34] O. Majoulet, C. Salameh, M.E. Schuster, U.B. Demirci, Y. Sugahara, S. Bernard, P. Miele, Synthesis of periodic mesoporous silicon-aluminium-carbon-nitrogen frameworks surface-decorated with Pt nanoparticles, Chem. Mater. 25 (2013) 3957–3970.
[35] F. Aldinger, M. Weinmann, J. Bill, Precursor-derived Si-B-C-N ceramics, Pure Appl. Chem. 70 (1998) 439–448.
[36] M. Weinmann, J. Schuhmacher, H. Kummer, S. Prinz, J. Peng, H.J. Seifert, M. Christ, K. Müller, J. Bill, F. Aldinger, Synthesis and thermal behavior of novel Si-B-C-N ceramic precursors, Chem. Mater. 12 (2000) 623–632.
[37] N. Janakiraman, M. Weinmann, J. Schuhmacher, K. Müller, J. Bill, F. Aldinger, Thermal stability, phase evolution, and crystallization in Si-B-C-N ceramics derived from a polyborosilazane precursor, J. Am. Ceram. Soc. 85 (2002) 1807–1814.
[38] A.H. Tavakoli, P. Gerstel, J.-A. Golczewski, J. Bill, Effect, of boron on the crystallization of amorphous Si-(B-)C-N polymer-derived ceramics, J. Non-Cryst. Solids 355 (2009) 2381–2389.
[39] A. Müller, P. Gerstel, M. Weinmann, J. Bill, F. Aldinger, Correlation of boron content and high temperature stability in Si-B-C-N ceramics, J. Eur. Ceram. Soc. 20 (2000) 2655–2659.
[40] A. Müller, P. Gerstel, M. Weinmann, J. Bill, F. Aldinger, Correlation of boron content and high temperature stability in Si-B-C-N ceramics, J. Eur. Ceram. Soc. 21 (2001) 2171–2177.
[41] T. Wideman, K. Su, E.E. Remsen, G.A. Zank, L.G. Sneddon, Synthesis, characterisation, and ceramic conversion reactions of borazine/silazane copolymers — new polymeric precursors to sincb ceramics, Chem. Mater. 7 (1995) 2203–2212.
[42] A. Viard, D. Fonblanc, M. Schmidt, A. Lale, C. Salameh, A. Soleilhavoup, M. Wynn, P. Champagne, S. Cerneaux, F. Babonneau, G. Chollon, F. Rossignol, C. Gervais, S. Bernard, Chem. Eur J. 23 (2017) 9076–9090.
[43] H. Termoss, B. Toury, S. Payan, A. Brioude, S. Bernard, D. Cornu, S. Vallette, S. Benayoun, P. Miele, Preparation of boron nitride-based coatings on metallic substrates via infrared irradiation of dip-coated polyborazylene, J. Mater. Chem. 19 (2009) 2671–2674.
[44] H.J. Seifert, H.L. Lukas, F. Aldinger, Development of Si-B-C-N ceramics supported by phase diagrams and thermochemistry, Ber. Bunsenges. Phys. Chem. 102 (1998) 1309–1313.
[45] M. Weinmann, R. Haug, J. Bill, M. De Guire, F. Aldinger, Boron-modified polysilylcarbodi-imides as precursors for Si-B-C-N ceramics: synthesis, plastic-forming and high-temperature behavior, Appl. Organomet. Chem. 12 (1998) 725–734.
[46] J. Bill, J. Seitz, G. Thurn, J. Dürr, J. Canel, B. Janos, A. Jalowiecki, D. Sauter, S. Schempp, P. Lamparter, J. Mayer, F. Aldinger, Structure analysis and properties of Si-C-N ceramics derived from polysilazanes, Phys. Status Solidi 166 (1998) 269–296.
[47] H. Dean Batha, E. Dow Whitney, Kinetics and mechanism of the thermal decomposition of Si_3N_4, J. Am. Ceram. Soc. 56 (1973) 365–369.
[48] H.P. Martin, E. Müller, G. Irmer, F. Babonneau, Crystallization behaviour and polytype transformation of polymer-derived silicon carbide, J. Eur. Ceram. Soc. 17 (1997) 659–666.
[49] Y. Li, L. Wang, S. Yin, F. Yang, Crystallization behaviour of amorphous silicon nitride added with silicon powder, Mater. Chem. Phys. 141 (2013) 874–881.
[50] Z. Li, W. Zhou, X. Su, F. Luo, Y. Huang, C. Wang, Effect of boron doping on microwave dielectric properties of SiC powder synthesized by combustion synthesis, J. Alloys Compd. 509 (2011) 973–976.
[51] M. Gadzira, G. Gnesin, O. Mykhaylyk, O. Andreyev, Synthesis and structural peculiarities of non-stoichiometric beta-SiC, Diam. Relat. Mater. 7 (1998) 1466–1470.
[52] O. Hod, Graphite and hexagonal boron-nitride have the same interlayer distance, Why? J. Chem. Theory Comput. 8 (2012) 1360–1369.
[53] S. Bernard, F. Chassagneux, M.-P. Berthet, D. Cornu, P. Miele, Crystallinity, crystalline quality and microstructural ordering in boron nitride fibers, J. Am. Ceram. Soc. 88 (2005) 1607–1614.
[54] Z.D. Zujovic, R. Etzion, J.B. Metson, Solid-State NMR characterisation of silicon nitride bonded silicon carbide refractories, Ind. Eng. Chem. Res. 47 (2008) 9913–9918.
[55] O. Majoulet, J.G. Alauzun, L. Gottardo, C. Gervais, M.E. Schuster, S. Bernard, P. Miele, Ordered mesoporous silicoboron carbonitride ceramics from boron-modified Polysilazanes: polymer synthesis, processing and properties, Micro, Meso. Mater. 140 (2011) 40–50.
[56] C. Gervais, F. Babonneau, L. Ruwisch, R. Hauser, R. Riedel, Solid state NMR investigations oft he polymer route to SiBCN ceramics, Can. J. Chem. 81 (2003) 1–11.
[57] J. Seitz, J. Bill, N. Egger, F. Aldinger, Structural investigations of Si/C/N-ceramics from polysilazane precursors by nuclear magnetic resonance, J. Eur. Ceram. Soc. 16 (1996) 885–891.
[58] F. Berger, A. Müller, F. Aldinger, K. Müller, Solid-state NMR investigations on Si-B-C-N ceramics derived from boron- modified poly(allylmethylsilazane), Z. Anorg. Allg. Chem. 631 (2005) 355–363.
[59] G. Schumacher, F. Berger, M. Weinmann, J. Bill, F. Aldinger, K. Muller, Solid-state NMR and FT IR studies oft he preparation of Si-B-C-N ceramics from boron-modified polysilazanes, Appl. Organomet. Chem. 15 (2001) 809–819.
[60] L. Gottardo, S. Bernard, C. Gervais, M. Weinmann, P. Miele, Study of the intermediate pyrolysis steps and mechanism identification of polymer-derived SiBCN ceramics, J. Mater. Chem. 22 (2012) 17923–17933.
[61] L. Gottardo, S. Bernard, C. Gervais, K. Inzenhofer, G. Motz, M. Weinmann, C. Balan, P. Miele, Chemistry, structure and processability of boron-modified polysilazanes as tailored precursors of ceramic fibers, J. Mater. Chem. 22 (2012) 7739–7750.
[62] N. Wada, S. Solin, J. Wong, S. Prochazka, Raman and IR absorption spectroscopic studies on α, β and amorphous Si_3N_4, Non-Cryst. Solids 43 (1981) 7–15.